Responses to Anonymous Referee #1's comments (RC1):

Thanks are extended to the Professor, Markku Kulmala, and to the two anonymous Referees, for their careful work and thoughtful and very important suggestions that greatly improve the manuscript.

The following text contains the Referees' comments (black), our replies (blue) and the changes made to the manuscript (red).

Comment 01: The paper shows the observation of 3D electric field in dust storms. However, the characteristics of 3D electric field has been reported in another paper of the author (Atmos. Chem. Phys., 18, 17087–17097, 2018.), thus, "...performed the first-ever measurements of 3D E-field…" is questionable.

Response:

According to your suggestion, the statements related to "first-ever measurements", such as "...performed the first-ever measurements of 3D E-field…" have been modified as follows:

"…In this study, we performed the field measurements of 3-D E-field in the sub-meter layer from 0.05 to 0.7 m above the ground during dust storms by VREFM sensors…" Please see page 25 lines 25-27 in the revised manuscript (MS) for details.

"5.1. Field measurements of 3-D E-field in the sub-meter layer" Please see page 22 line 5 in the revised MS for details.

In fact, in our previous study (Atmos. Chem. Phys., 18, 17087–17097, 2018.), the E-field measurements were performed at approximately 5 m height, where the suspension motion dominates. In contrast, in this study, we measured E-field in the sub-meter region (below 1 m height), where the saltation motion dominates. Therefore, the properties of E-field are quite different in these two regions.

Comment 02: In this manuscript, the observation values are decomposed into streamwise E-field, spanwise E-field and vertical E-field by mathematical method. However, the manuscript does not explain why streamwise E-field and spanwise E-field happens, and why are they an order of magnitude larger than the vertical electric field? The effects of streamwise E-field and spanwise E-field on sand saltation are not clearly explained. In fact, this should be the highlight of this manuscript.

Response:

According to your suggestion, we have added a possible explanation of why the streamwise and spanwise E-fields happens, and why they are larger than the vertical E-field:

"… In contrast to the vertical component, which is closely related to the total mass loading (Esposito et al., 2016; Williams et al., 2009), the intense streamwise and spanwise components are aerodynamically created due to the nonuniform transport of charged particles in the streamwise and spanwise directions (Zhang et al., 2014). It is well-known that dust storm is a polydisperse particle-laden turbulent flow at very high-Reynolds-number (up to ~108). During dust storms, the particle transport is regulated by the large- and very-large-scale motions of wind flows (Jacob and Anderson, 2016), which may lead to the phenomenon that the charged particles are more nonuniformly distributed (over a larger spatial scale) in dust storms than in pure saltation…" Please see page 23 lines 16-25 in the revised MS for details.

In the revised MS, the effects of streamwise and spanwise E-fields on mass flux and saltation height have been discussed and explained in details. The main revision in the revised MS are given as follows:

"By substituting the formulations of the 3-D E-field (i.e. $\langle\overline{E_i}\rangle E_i^+$, $i = 1,2,3$) into our model (i.e. Eq. 10a), we then evaluate the effects of 3-D E-field on saltation during storms properly. As shown in Fig. 8a, compared to the case without E-field, the vertical component of the E-field (i.e. 1-D E-field) inhibits mass flux, in agreement with previous studies (Kok and Renno, 2008; Zheng et al., 2003). However, the mass flux is

enhanced by 3-D E-field, causing the simulated value closer to our measured data. Such enhancement of mass flux by 3-D E-field can be qualitatively explained by the considerable enhancements of m_c below ~0.02 m height (Fig. 9a) and $\langle u_p \rangle$ in the range from 0.01 to 0.1 m height (Fig. 9b), due to the streamwise and spanwise components. Meanwhile, although the saltation height is not sensitive to E-field vertical component, 3-D E-field enhances the saltation height significantly and, therefore, makes the numerical prediction more accurate (Fig. 8b). This is because when considering the E-field vertical component, the mass flux profile is very similar to the case of no E-field consideration (Figs. 8a and 9). In contrast, 3-D E-field causes a distortion of the mass flux profile (as well as m_c and $\langle u_p \rangle$), and thus alters saltation height significantly (Figs. 8a and 9).

Additionally, we also explore how the key parameter, density of charged species ρ_h^0, affects saltation, as shown in Figs. 10a-10c. Since the height-averaged time-varying mean is strongly depended on the ambient conditions such as temperature and RH, the height-averaged time-varying mean is set at two different levels. The predicted results show that, at each height-averaged time-varying mean level, the magnitude of the charge-to-mass ratio increases with increasing ρ_h^0, and then reaches a relatively equilibrium value at approximately $\rho_h^0 = 10^{16}$ m^{-2} (Fig. 10a), thus leading to a constant enhancement of total mass flux Q and saltation height z_{salt} (Figs. 10b and 10c). For the larger height-averaged time-varying mean, the enhancements of the total mass flux Q and saltation height z_{salt} could exceed 20 % and 15 %, respectively." Please see pages 21-22, lines 6-29 in page 21 and lines 1-2 in page 22, in the revised MS for details.

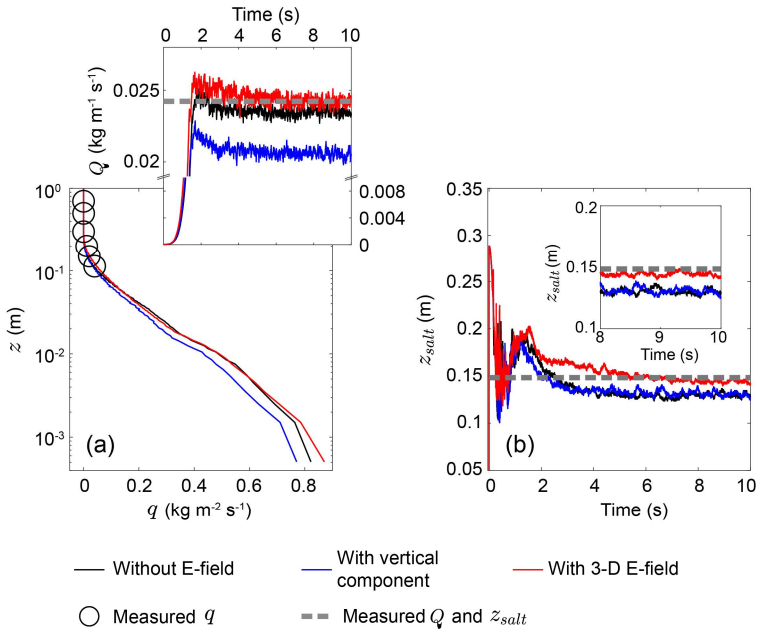

Figure 8. Comparison of the simulated mass flux q and total mass flux Q (a) and saltation height z_{salt} (b) with our measurements in the relatively steady period of the observed dust storm (shaded in Fig. 4 and Fig. S3 in the Supplement), where u_*=0.37 m s^{-1}, d_m=200 μm, σ_p=exp (0.42), ρ_h^0=6×10^{15} m^{-2}, and e_n=0.7. (a) Circles are the measured mean mass flux, dashed line denotes the estimated mean total mass flux, and lines denote the simulated results. (b) Dashed lines denote the estimated saltation height based on our measurements and lines denote simulated results. The uncertainty analysis of the measured or estimated results can be found in Text S1 in the Supplement.

Please see page 43 lines 2-11 in the revised MS for details.

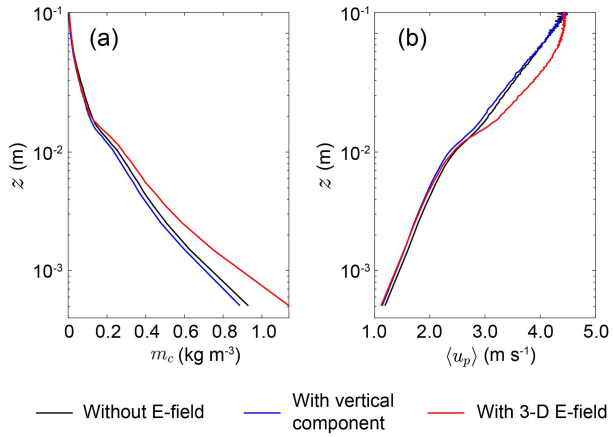

Figure 9. Vertical profiles of the particle mass concentration m_c and mean particle horizontal speed $\langle u_p \rangle$ for different cases, where u_*=0.37 m s^{-1}, d_m=200 μm, σ_p=exp(0.42), ρ_h^0=6×10^{15} m^{-2}, and e_n=0.7.

Please see page 44 lines 2-5 in the revised MS for details.

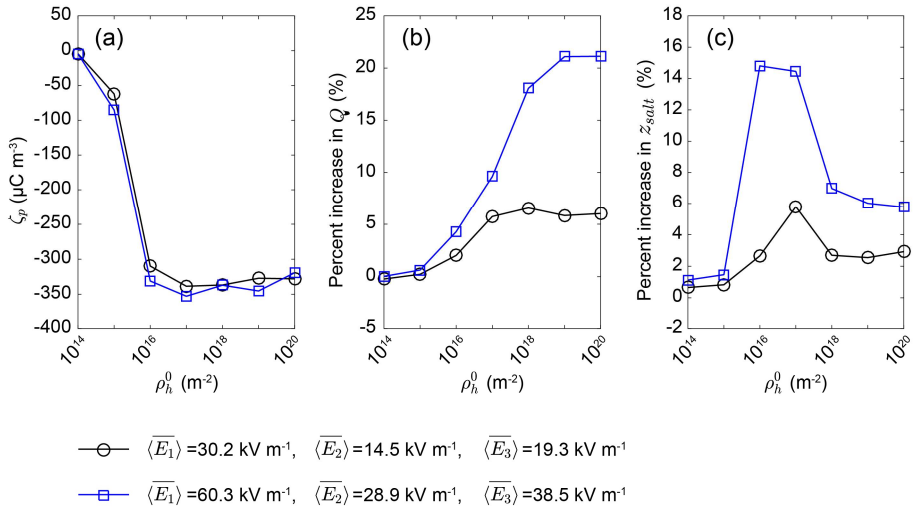

Figure 10. Effects of the density of charged species ρ_h^0 on saltation for two different height-averaged time-varying mean levels (i.e. $\langle\overline{E_i}\rangle$, $i = 1,2,3$). (a) The mean charge-to-mass ratio ζ_p (in the range from 0.07 to 0.09 m height) as a function of ρ_h^0 ranging from 10^{14} to 10^{20} m^{-2} (e.g. Kok and Lacks, 2009). (b) Percent increase in the total mass flux Q as a function of ρ_h^0. (c) Percent increase in the saltation height z_{salt} as a function of ρ_h^0. The squares correspond to the height-averaged time-varying mean in the steady stage of the observed dust storm (shaded in Fig. S7 in the Supplement). In these cases, e_n=0.7.

Please see page 45 lines 2-10 in the revised MS for details.

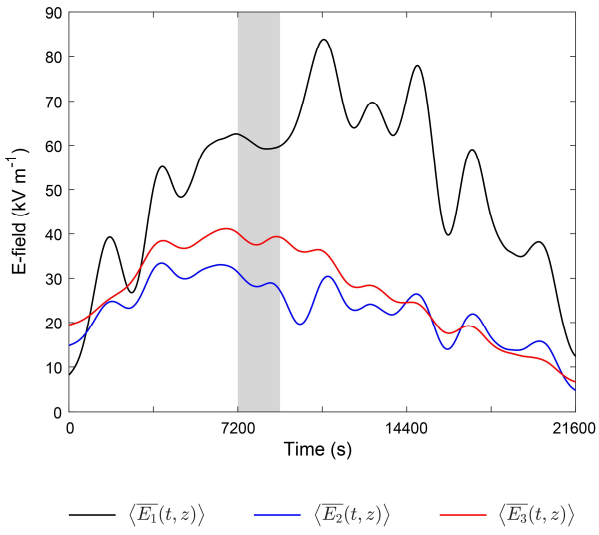

Figure S7. The height time-varying mean series of the 3-D E-field. The shaded area denotes the relatively steady period of the observed dust storms. Times are shown relative to May 6, 2014 at 13:00:00 UTC+8.

Please see page 11 in the revised Supplement for details.

Comments 03: In Section 3.2, how to determine the value of charge-to-mass ratio? Is a specified value, or the charges generated by sand particles collision, in fact, the charges generated by the collision of 100 uncharged particles in the calculation domain should be very small.

Response:

In our model, particles' charge is changed after every collision, which is calculated by Eqs. (24) and (25) in the revised MS. Therefore, the instantaneous charge-to-mass ratio equals to the ratio of particle's instantaneous charge to its mass. To make the reader better understanding the determination of charge-to-mass, the following descriptions have been added in the revised manuscript:

"…$\zeta_{p,i}$ is the charge-to-mass ratio of the sand particles and will be altered during every collision (see section 3.4) …" Please see page 11 lines 1-2 in the revised MS for details.

"…If the particle's net electrical charge is known, its charge-to-mass ratio can be easily determined." Please see page 17 lines 6-7 in the revised MS for details.

Our model is initiated by randomly releasing 100 uncharged particles. Subsequently, the impact particles will eject more particles into the air (Fig. R1), this process is quantificationally described in section 3.3 in the manuscript.

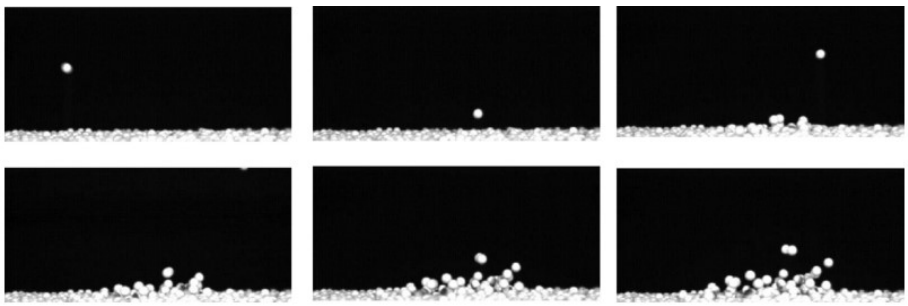

Figure R1. High-speed images of the splashing of surface particles by an impacting saltating particle; the time step between two successive images is 4 ms (Kok et al., 2012).

Therefore, the total number of saltating particles is actually more than 7×10^4 when the wind friction velocity u_* is 0.5 m s^{-1}. In the revised MS, we have showed the evolution of the total number of saltating particles in Fig. S8 in the Supplement, that is:

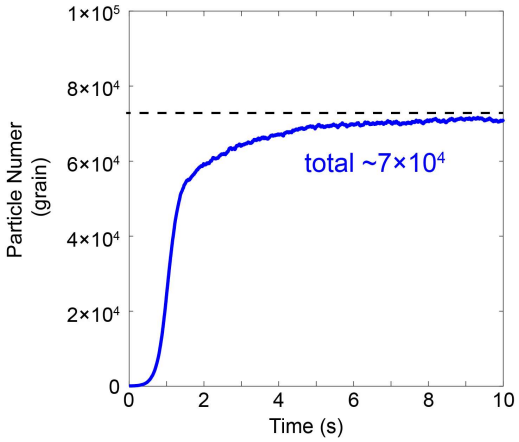

Figure S8. The total number of saltating particles in the case of Fig. 6 in the manuscript.

Please see page 12 in the revised Supplement for details.

Comments 04: In Section 3.2.1, the effect of turbulence on the movement of sand particles does not consider in severe dust storm, which obviously affects the charged characteristics of sand particles and electric field distribution in dust storm.

Response:

Indeed, turbulence plays a key role in saltation, especially for large wind speed (Kok et al., 2012). However, saltation is polydisperse particle-laden turbulent flows at a very high-Reynolds-number (up to ~10^8), which needs huge computational cost to resolve the turbulent fluctuations, even though we use large-eddy simulation. On the other hand, to account for particle triboelectric charging, the particle-scale simulation (i.e. discrete element method) is needed. As discussed in comment 03, the number of saltating particles is often on the order of 10^5. The discrete element method simulation of particle triboelectric charging is also computationally expensive.

In this study, we are mainly concerned with the first-order statistics (thus do not assess higher-order statistics), and therefore the calculation of the wind field is

simplified to Eq. (12) in the manuscript, which is based on the mixing length theory (please see Chapter 6 in Shao, 2008 for details).

In the revised manuscript, we have discussed the importance of turbulence as follows:

"…However, a remaining critical challenge is still to simulate particle triboelectric charging in dust storms precisely. The driving atmospheric turbulent flows having a typical Reynolds number on the order of 10^8 cover a broad range of length and time scales, which needs huge computational cost to resolve (e.g. Shao, 2008). On the other hand, particle triboelectric charging is so sensitive to particle's collisional dynamics that it needs to resolve each particle collisional dynamics (e.g. Hu et al., 2012; Lacks and Sankaran, 2011). To model the particle's collisional dynamics properly, the time steps of DEM are generally from 10^{-7} to 10^{-4} s (Norouzi et al., 2016). However, steady-state saltation motion often requires several seconds to several tens of seconds to reach the equilibrium state. In this study, when $u_* = 0.5$ m s^{-1} and the computational domain is 0.5×0.1×1.0 m^3, the total number of saltating particles exceeds 7×10^4 (Fig. S8 in the Supplement). Consequently, the triboelectric charging in saltation is currently very difficult to simulate, where a large number of polydisperse sand particles, the high Reynolds-number turbulent flow, and the inter-particle electrostatic forces are mutually coupled. In the present version of the model, we do not consider the particle-particle interactions such as particle agglomeration and fragmentation during particle collision or frictional contact, as well as the particle-turbulence interaction that is the effects of turbulent fluctuations on the triboelectric charging and dynamics of particles. Further studies require considerable effort to incorporate these interactions, especially turbulence, which is very important for large wind velocity." Please see page 25 lines 1-20 in the revised MS for details.

"…A great effort is further needed to understanding the interactions such as particle agglomeration and fragmentation, as well as the effects of the turbulence on

the triboelectric charging and dynamics of particles." Please see page 26 lines 14-16 in the revised MS for details.

Comments 05: In Section 3.4, how to determine the value of rho(hj), the value adopted in the model should be given.

Response:

The following description of ρ_h^j has been added in the revised MS:

"…ρ_h^i is the density of the electrons trapped in the high energy states on the surface of particle i (assuming that all particles have an identical initial value ρ_h^0), which is modified as $\rho_{h,i}^{\text{after}} = \rho_{h,i}^{\text{before}} + (\rho_h^j S_j - \rho_h^i S_i)/(\pi d_i^2)$ due to collisions between particle i and j;…" Please see page 16 lines 20-23 in the revised MS for details.

Comments 06: Section 3.5, about the computational domain 0.5 m × 0.1 m × 1.0 m, the electric field in the x and y directions is an order of magnitude larger than the z direction, while the length in the y direction in the calculation region is only 0.1 m, although periodic boundary conditions are set, the particle collision characteristics have changed.

Response:

Thanks for your very useful suggestions. We are very sorry for our inappropriate statement, i.e. "*…it can be seen that, in general, the streamwise component (up to ~80 kV m^{-1}) and spanwise component (up to ~60 kV m^{-1}) are one order of magnitude larger than the vertical component of the E-field (~7 kV m^{-1})…*", in the original manuscript. The magnitude of the vertical E-field is incorrectly labeled in the old version of Fig. 4. In fact, the magnitude of the vertical E-field is as large as ~40 kV m^{-1}, which can be checked in any version of the provided data file 'ds01.csv'. Thus, the new version of Fig. 4 in the revised manuscript is modified as follows:

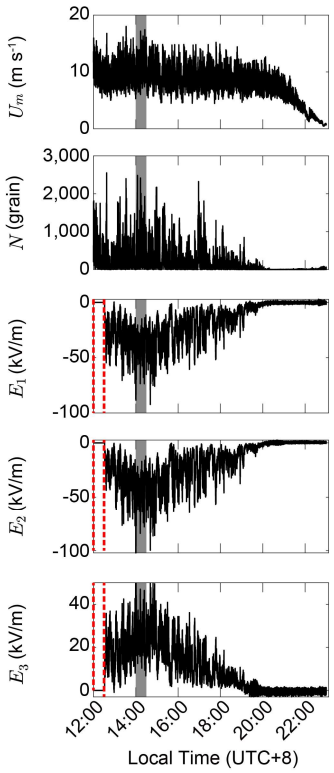

Figure 4. Measured results during a dust storm occurring on May 6, 2014, at the QLOA site. (a)-(e): the measured time series of the streamwise wind speed, u_m at 0.7 m; the number of saltating particle N at 0.15 m; streamwise E-field E_1, spanwise E-field E_2, and vertical E-field E_3 at 0.7 m. Unfortunately, owing to the interruption of power supply, the 3-D E-field data have not been recorded before ~12:30, as represented by a dashed box in the last three panels (from top to bottom). The shaded area denotes the relatively stationary period of the observed dust storm.

Please see page 39 lines 2-9 in the revised MS for details.

Meanwhile, the related statements have been modified as:

"… From Fig. 4, it can be seen that, in general, the streamwise and spanwise components (up to ~80 kV m^{-1}) are consistently larger than the vertical component of the E-field (up to ~40 kV m^{-1}) …" Please see page 19 lines 11-13 in the revised MS for details.

In addition, the reason of the selection of the spanwise computational dimension is given in the revised manuscript:

"… To reduce the computational cost, the spanwise dimension is chosen as $L_y = 0.1$, since the saltating particles are mainly moving along the streamwise direction …" Please see page 18 lines 5-7 in the revised MS for details.

In our model, the periodic collision search algorithm is applied, which may slightly alter the particle collision characteristics. For example, for the particles in the right edge cell (target cell labeled by #4), in addition to cells #3 and #4, the collision searches are also performed over the particles in the left edge neighboring cell #1.

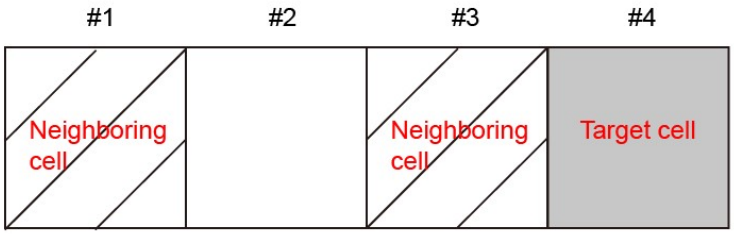

Figure R2. The periodic boundary conditions used in our model.

Comments 07: Fig. 5(c), the author should give the reason for vertical component E_3* increases monotonically as height increases in the saltation layer.

Response:

The property of the 3-D E-field in the saltation layer is strongly depended on the determination of the saltation height. For example, if the saltation height is 0.7 m, all measurement points (0.05-0.7 m height) is located in the saltation layer. In this case, the 3-D E-field exhibited a nonmonotonic pattern; that is, the vertical component decreases first, then increases, and decreases again, as height increases. In contrast, if the saltation height is less than 0.3 m, there exist only two measurements points (0.05 and 0.15 m height) in the saltation layer. In this case, the fitted curve of vertical component decreases monotonically with increasing height when z^+ is less than 1.

In fact, the determination of the saltation height is highly sensitive to the computational method. In the revised manuscript, following the methods of Martin and Kok (2017) and Sherman and Li (2012), we recalculate the saltation height within every 30 minutes time window, and thus the saltation height is found to be 0.172 ± 0.0343 m. This leads to only two measurement points in the saltation layer and the conclusion of "… vertical component E_3* increases monotonically as height increases in the saltation layer …" is no longer satisfied. In addition, the time-varying means of

the measured E-field series are extracted by the discrete wavelet transform (DWT) method (Daubechies, 1990) and ensemble empirical mode decomposition (EEMD) method (Wu and Huang, 2009). Therefore, the new version of Fig. 5 in the manuscript is as follows:

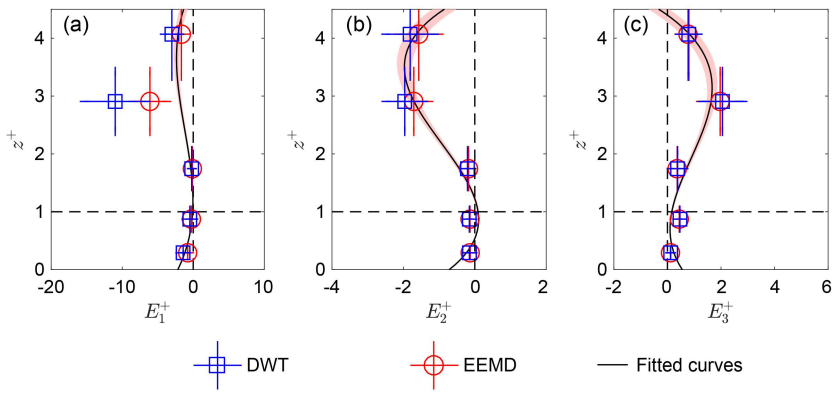

Figure 5. Vertical profiles of the normalized 3-D E-field. Subgraphs (a)-(c), in turn, correspond to the vertical profiles of E_1^+, E_2^+, and E_3^+ of the observed dust storm. Squares and circles denote the DWT mean and EEMD mean values of the normalized E-field data, respectively. Error bars are standard deviations. Lines denote robust linear least-squares fitting of the normalized E-field data obtained by DWT and EEMD method using 3-order polynomials (with R^2 of 0.97, 0.80, and 0.67, respectively), where the shaded areas denote 95% confidence bounds.

Please see page 40 lines 2-9 in the revised MS for details.

In the revised manuscript, the statement of "… vertical component E_3* increases monotonically as height increases in the saltation layer …" has been modified as:

"… Interestingly, Fig. 5c shows that during dust storms, all normalized components, E_1^+ to E_3^+, decreases monotonically as height increases in the saltation layer (i.e. $z^+ \leq 1$), similar to the pattern of vertical component in pure saltation…" Please see page 19 lines 21-23 in the revised MS for details.

The detailed calculation of the saltation height and its uncertainty analysis are provided in Text S1 in the Supplement:

"In our field campaign, we measured the saltating particle number flux at 6 heights from 0.05 to 0.7 m. Thus, the mass flux at each measurement height can be reasonably estimated by

$$q(z) = \frac{\pi \rho_p}{6 L_x L_y T_w} \sum_{i=1}^{n} (N_i d_i^3) \tag{s2}$$

Note that the summation $\sum$ is performed for the particles located in the range of $[z, z + \Delta z]$ over the 30-min time windows (i.e., T_w=30 minutes), in order to collect sufficient sand samples and capture the full range of turbulent fluctuations (e.g. Martin and Kok, 2017; Sherman and Li, 2012). Since SPC-91 measures the particle diameter with an uncertainty of $\Delta d = \pm 0.015$ mm (see SPC-91 Installation Guide, Niigata Electric Co., Ltd. for details), the uncertainty of estimating mass flux is $\Delta q \sim 3 d^2 \Delta d$ (i.e. $q \sim d^3 \Rightarrow \Delta q \sim 3 d^2 \Delta d$). As shown in Fig. S2, the measured mass flux data during different time intervals can be well fitted by the exponential functions (Shao, 2008):

$$q(z) = q_0 \exp(-az) \tag{s3}$$

where q_0 is the value of q at $z = 0$ and a is a positive empirical constant. Hence, the total mass flux can be determined by

$$Q = \int_0^{+\infty} q(z) dz = \frac{q_0}{a} \tag{s4}$$

Similarly, the uncertainty of the total mass flux is

$$\Delta Q = \frac{a \Delta q_0 - q_0 \Delta a}{a^2} \tag{s5}$$

Additionally, the saltation height, which is defined as the height below which 99 % of the total mass flux is present, can be given by (Dupont et al., 2013; Kok et al., 2012)

$$\int_0^{z_{salt}} q(z)dz = \frac{0.99q_0}{a} \tag{s6a}$$

$$\Rightarrow z_{salt} = -\frac{\ln(0.01)}{a} \tag{s6b}$$

Similarly, the uncertainty of the saltation height is

$$\Delta z_{salt} = -\frac{\ln(0.01)}{a^2}\Delta a \tag{s7}$$

As shown in Fig. S3, the estimated saltation height slightly varies with time, and thus we use the mean saltation height, which is 0.172 $\pm$ 0.0343 m, to obtain the dimensionless height z^+. For different time windows (i.e. T_w =5, 10, 30 minutes), there is no obvious differences between the mean values of Q and z_{salt}, but the standard deviations decrease as T_w increases (Fig. S3)." Please see pages 2-4 in the revised Supplement for details.

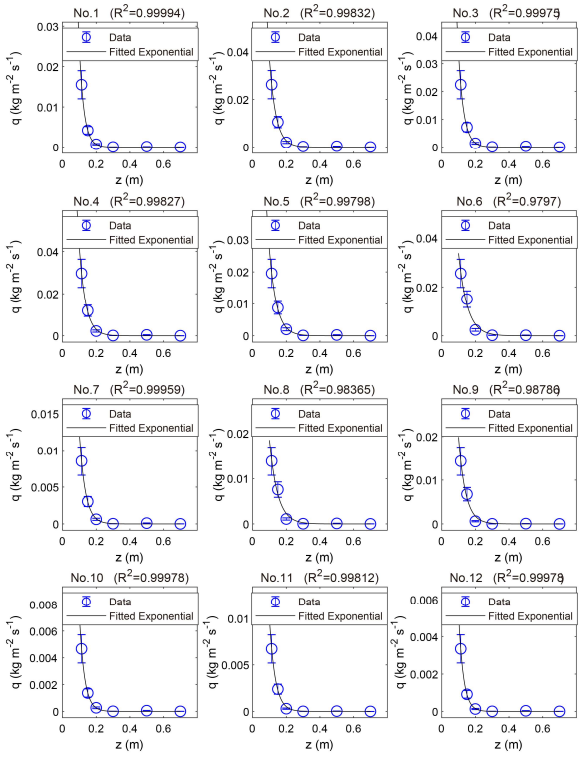

Figure S2. An example of the estimation of the total mass flux Q and saltation height z_{salt} in this

study, where No. i corresponds to time interval of $[(i-1)T, iT]$. The measured mass flux data are fitted by the exponential function $q(z) = q_0 \exp(-az)$, with R^2 larger than 0.9. Thus, the total mass flux and saltation height can be estimated by Eqs. s4-s7 in the Supplement, respectively.

Please see page 6 in the revised Supplement for details.

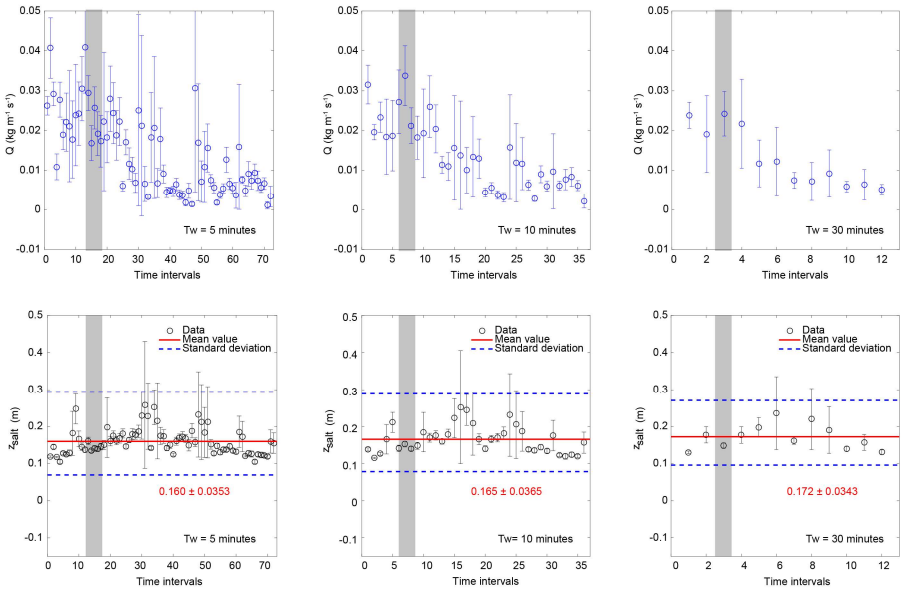

Figure S3. The estimated total mass flux Q (upper panels) and the saltation height z_{salt} (lower panels) with different time windows T_w (i.e. 5, 10, and 30 minutes) using the methods described in the Text S1. In the lower panels, the horizontal lines (in red) denote the mean saltation height, and the horizontal dashed lines (in blue) denote standard deviation. The shaded areas denote the relatively steady period of the observed dust storm.

Please see page 7 in the revised Supplement for details.

Comments 08: The boundary conditions in the simulation are not exactly the same as those in the observations. Section 4.1, the author should give a calculation method of the total mass flux in the simulation.

Response:

In the revised manuscript, we have added the calculations of some particle statistics, including the total mass flux, particle mass concentration, and mean particle horizontal speed, that is:

"3.5 Particle-phase statistics

Similar to particle momentum flux (i.e. Eq. 13), particle horizontal mass flux q, total mass flux Q, mean particle mass concentration m_c, and mean particle

horizontal speed $\langle u_p \rangle$ can be numerically determined by (Carneiro et al., 2013; Dupont et al., 2013)

$$q(z) = \frac{\sum m_{p,i} u_{p,i}}{L_x L_y \Delta z} \tag{26a}$$

$$Q = \frac{\sum m_{p,i} u_{p,i}}{L_x L_y} \tag{26b}$$

$$m_c(z) = \frac{\sum m_{p,i}}{L_x L_y \Delta z} \tag{26c}$$

$$\langle u_p \rangle(z) = \frac{\sum u_{p,i}}{L_x L_y \Delta z} \tag{26d}$$

where the summation $\sum$ is performed over the saltating particles located in the range of $[z, z + \Delta z]$ for q, m_c, and $\langle u_p \rangle$, but it is performed over all saltating particles for Q." Please see page 17 lines 9-22 in the revised MS for details.

Comments 09: Section 4.3, the conclusion of "3-D E-field enhances the total mass flux even up to ~63%" is not sufficient. The manuscript does not give the basis for lambda(i), and the meaning of specified value of lambda(i) in Figure 9(b) is also not clear.

Response:

In the original manuscript, λ is, in fact, the height-averaged time-varying mean of the E-field $\langle \overline{E_i} \rangle$, which is clearly defined by Eq. 5 in the revised manuscript. To eliminate the ambiguous meaning of λ, we directly regard the height-averaged time-varying mean as a basic parameter (therefore, λ has been removed in the revised manuscript). When exploring the effects of the density of charged species ρ_h^0 on saltation, we set $\langle \overline{E_i} \rangle$ at two different levels; that is, it equals to $0.5\langle \overline{E}_{\text{steady}} \rangle$ and $\langle \overline{E}_{\text{steady}} \rangle$, where $\langle \overline{E}_{\text{steady}} \rangle$ denotes the height-averaged time-varying mean during the steady period of the observed dust storm (depicted by the shaded area in Fig. 4 in

the revised manuscript). The selection of $\langle\overline{E_i}\rangle$ is based on the fact that E-field is strongly depended on the ambient conditions such as temperature and relative humidity. At given particle concentration, the E-field could vary with the temperature and relative humidity (Esposito et al., 2016; Zhang and Zheng, 2018). In the revised manuscript, we find that the enhancement of the total mass flux Q and saltation height z_{salt} could exceed 20 % and 15 %, respectively, when the height-averaged time-varying mean $\langle\overline{E_i}\rangle$ equals $\langle\overline{E}_{\text{steady}}\rangle$. The main revision associated with this comment are as follows:

"…Additionally, we also explore how the key parameter, density of charged species ρ_h^0, affects saltation, as shown in Figs. 10a-10c. Since the height-averaged time-varying mean is strongly depended on the ambient conditions such as temperature and RH, the height-averaged time-varying mean is set at two different levels. The predicted results show that, at each height-averaged time-varying mean level, the magnitude of the charge-to-mass ratio increases with increasing ρ_h^0, and then reaches a relatively equilibrium value at approximately $\rho_h^0 = 10^{16}$ m^{-2} (Fig. 10a), thus leading to a constant enhancement of total mass flux Q and saltation height z_{salt} (Figs. 10b and 10c). For the larger height-averaged time-varying mean, the enhancements of the total mass flux Q and saltation height z_{salt} could exceed 20 % and 15 %, respectively." Please see pages 21-22, lines 22-29 in page 21 and lines 1-2 in page 22, in the revised MS for details.

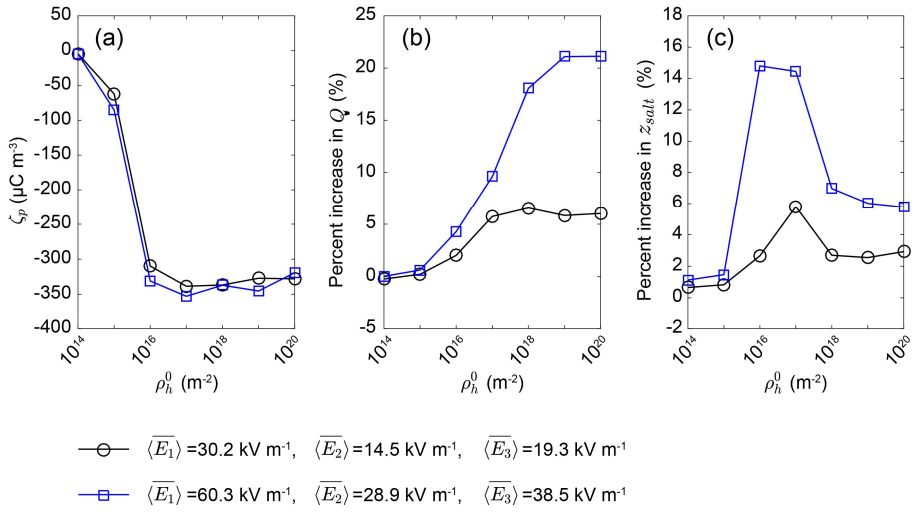

Figure 10. Effects of the density of charged species ρ_h^0 on saltation for two different height-averaged time-varying mean levels (i.e. $\langle\overline{E_i}\rangle$, $i = 1,2,3$). (a) The mean charge-to-mass ratio ζ_p (in the range from 0.07 to 0.09 m height) as a function of ρ_h^0 ranging from 10^{14} to 10^{20} m^{-2} (e.g. Kok and Lacks, 2009). (b) Percent increase in the total mass flux Q as a function of ρ_h^0. (c) Percent increase in the saltation height z_{salt} as a function of ρ_h^0. The squares correspond to the height-averaged time-varying mean in the steady stage of the observed dust storm (shaded in Fig. S7 in the Supplement). In these cases, e_n=0.7.

Please see page 45 lines 2-10 in the revised MS for details.

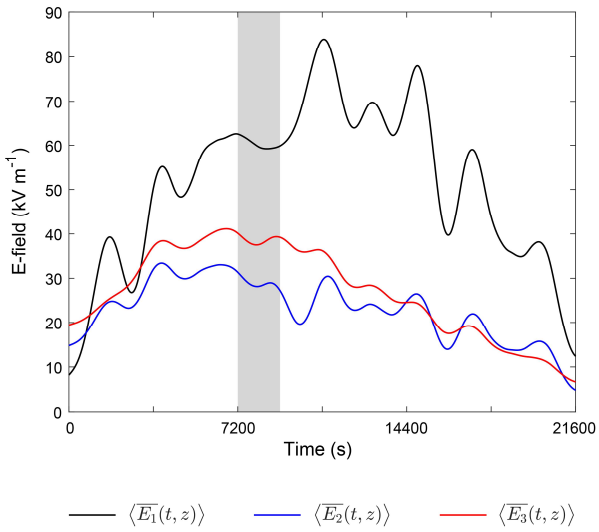

Figure S7. The height time-varying mean series of the 3-D E-field. The shaded area denotes the relatively steady period of the observed dust storms. Times are shown relative to May 6, 2014 at 13:00:00 UTC+8.

Please see page 11 in the revised Supplement for details.

Responses to Anonymous Referee #2's comments (RC2):

Thanks are extended to the Professor, Markku Kulmala, and to the two anonymous Referees, for their careful work and thoughtful and very important suggestions that greatly improve the manuscript.

The following text contains the Referees' comments (black), our replies (blue) and the changes made to the manuscript (red).

Comment 01: The authors used the empirical mode decomposition (EMD) to capture the time varying features in the measured 3D E-filed data. Similar tools also exist, such as the wavelet transformation. Why the authors chose EMD over the wavelet method? EMD is known to likely cause problems at the beginning and end of a time series. How did the authors deal with such issues? The application of EMD is also vulnerable to mode mixing. How was this problem handled in estimating the time-varying mean values?

Response:

As you pointed out that the EMD method in the original manuscript (MS) may cause the ending effects and mode mixing. In order to solve these issues, we use the discrete wavelet transform (DWT) (Daubechies, 1990) and the ensemble empirical mode decomposition (EEMD) methods (Wu and Huang, 2009) to extract the meaningful time-varying means over the approximately 17-min timescales, because these two methods can significantly reduce the ending effects and mode mixing (please see the references of Daubechies, 1990 and Wu and Huang, 2009 for details).

As shown in the revised MS, the 17-min time-varying means can be defined as the 10-th order approximation component of DWT or the summation of the last four EEMD component and the residual.

According to your suggestion, the following changes have been made in the revised MS:

"… Here, we use the discrete wavelet transform (DWT) method (Daubechies, 1990) and the ensemble empirical mode decomposition (EEMD) method (Wu and

Huang, 2009), which are widely used in various geophysical studies (e.g. Grinsted et al., 2004; Huang and Wu, 2008; Wu et al., 2011), to estimate the time-varying mean values of the measured non-stationary 3-D E-field data. We select these two methods since the DWT with higher orders of Daubechies wavelet (e.g. db10) and the EEMD can extract a reasonable and physically meaningful time-varying mean (Su et al., 2015). Each step for revealing the 3-D E-field pattern is described in detail as follows:

The DWT uses a set of mutually orthogonal wavelet basis functions, which are dilated, translated and scaled versions of a mother wavelet, to decompose an E-field series $E(t,z)$ into a series of successive octave band components (Percival and Walden, 2000), i.e.,

$$E(t,z) = \sum_{i=1}^{N} \psi_i(t,z) + \chi_N(t,z) \tag{1}$$

Where N is the total number of decomposition levels, $\psi_i(t,z)$ denotes the i-th level wavelet detail component, and $\chi_N(t,z)$ represents the N-th level wavelet approximation (or smooth) component. As N increases, the frequency contents become lower and thus the N-th level approximation component could be regarded as the time-varying mean values (e.g. Percival and Walden, 2000; Su et al., 2015). In this study, the DWT decomposition is performed with the Daubechies wavelet of order 10 (db10) at level 10, and thus the 10-th order approximation component can be defined as the time-varying mean:

$$\overline{E}(t,z) = \chi_{10}(t,z) \tag{2}$$

which reflect the averages of the $E(t,z)$ series over a scale of 2^{10} s (about 17.1 minutes).

On the other hand, according to the empirical mode decomposition (EMD) method, the time series $E(t,z)$ can be decomposed as (Huang et al., 1998)

$$E(t,z) = \sum_{i=1}^{N} \xi_i\,(t,z) + \eta_N(t,z) \qquad (3)$$

through a sifting process, where $\xi_i(t,z)$ $(i = 1, 2, \ldots, N)$ are the intrinsic mode functions (IMFs), and $\eta_N(t,z)$ is a residual (which is the overall trend or mean). To reduce the end effects and mode mixing in EMD, the EEMD method is proposed by Wu and Huang (2009). In EEMD, a set of white noise series, $w_j(t,z)$ $(j = 1,2, \ldots N_e)$, are added to the original signal $E(t,z)$. Then, each noise-added series is decomposed into IMFs followed by the same sifting process as in EMD. Finally, the i-th EEMD component is defined as the ensemble mean of the i-th IMFs of the total of N_e noise-added series (see Wu and Huang, 2009 for details).

In this study, the time-varying mean values $\overline{E}(t,z)$ can be alternatively defined as the sum of the last four EEMD components, $\xi_{10}(t,z)$ to $\xi_{13}(t,z)$, and the residual, $\eta_{13}(t,z)$, i.e.

$$\overline{E}(t,z) = \sum_{i=1}^{13} \xi_i(t,z) + \eta_{13}(t,z) \qquad (4)$$

which is approximately the 17.3 minutes (very close to the timescale of ~17.1 minutes used in DWT) or longer timescale variability trend (Wu et al., 2011), because the maximum mean frequency of the last four EEMD components is 5.78 $\times 10^{-2}$ Hz (see Figs. S5 and S6 in the Supplement for details).

According to the above definitions, the time-varying mean can be obtained by the DWT and EEMD methods over the timescale of about 17 minutes. As an example, Fig. 2 shows the results of db10 DWT analysis (Fig. 2b) and EEMD decompositions (Fig. 2c) for an E-field time series $E(t,z)$ in our field campaign. It can be seen that DWT and EEMD can properly capture the time-varying mean over the timescale of 17 minutes, with very little difference between the two methods." Please see pages 6-8 in the

revised MS for details.

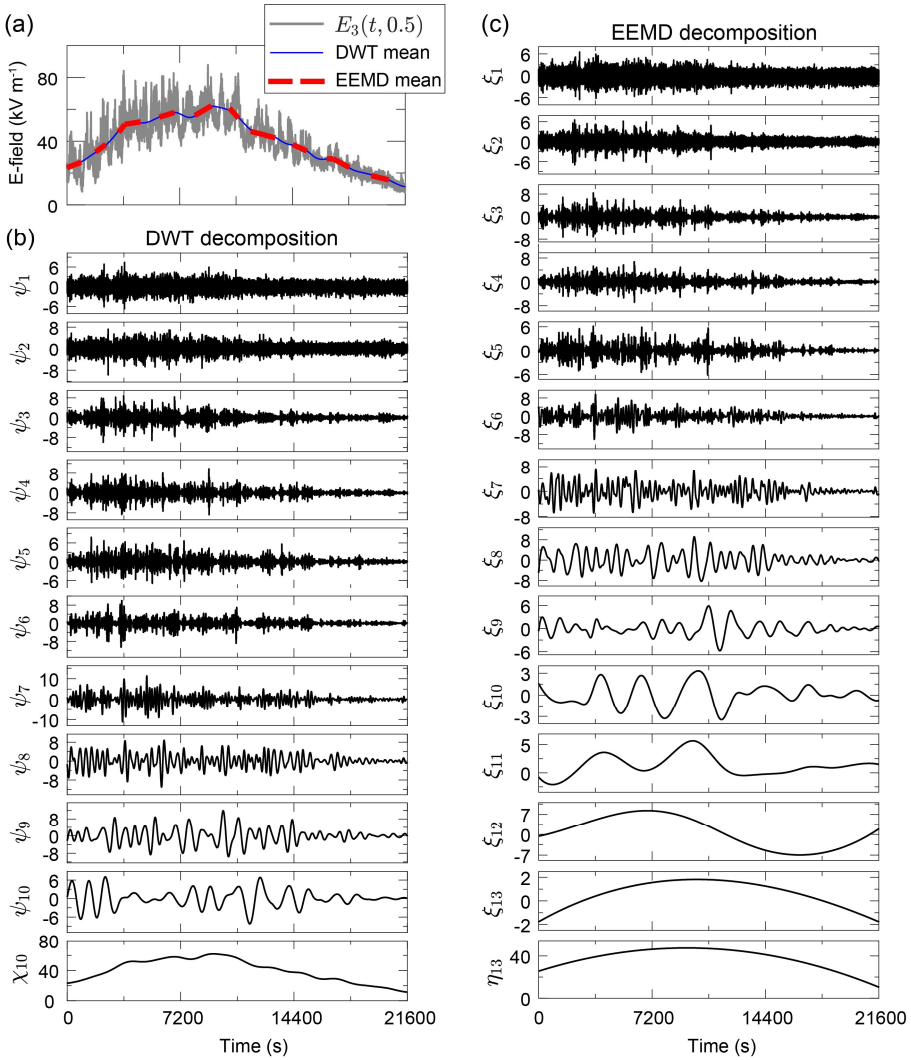

Figure 2. The resulting DWT and EEMD components from a measured vertical E-field component at 0.5 m height, $E_3(t, 0.5)$, with a total of N_d=21600 data points. (a) shows the original E-field time series (gray line), and the time-varying mean obtained by DWT (red line) and EEMD (blue dashed line). (b) shows the detailed components ψ_1-ψ_{10} and approximation component χ_{10} of DWT. (c) shows the EEMD components ξ_1-ξ_{13} and the residue η_{13}. In the EEMD, N is specified as $\log_2(N_d) - 1$, the member of ensemble N_e is 100, and the added white noise in each ensemble member has a standard deviation of 0.2. Times are shown relative to May 6, 2014 at 13:00:00 UTC+8.

Please see page 37 lines2-11 in the revised MS for details.

Additionally, in supplementary materials, the following changes have been made in the revised Supplement:

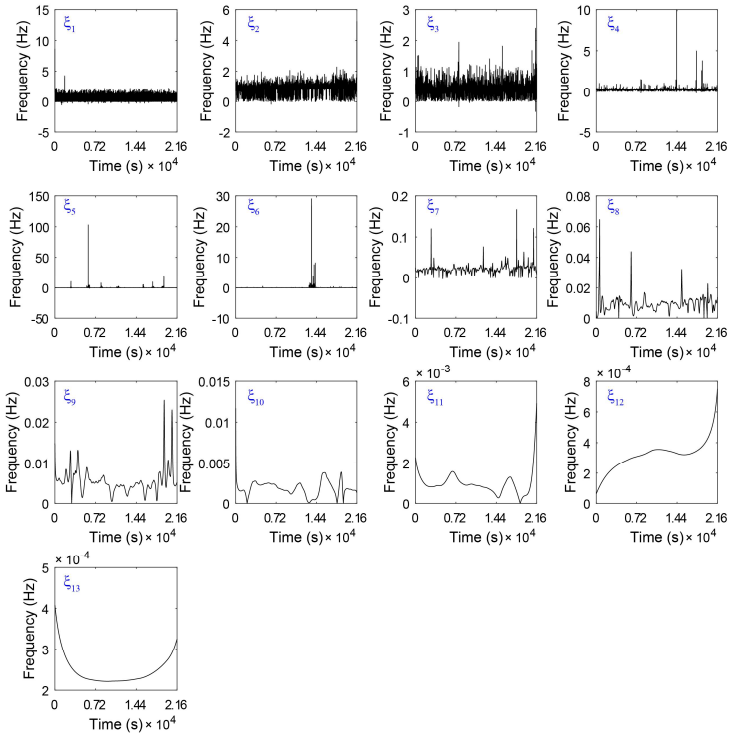

Figure S5. The instantaneous frequency of the EEMD components ξ_1-ξ_{13} for the vertical E-field series at 0.5 m height, i.e. $E_3(0.5)$.

Please see page 9 in the revised Supplement for details.

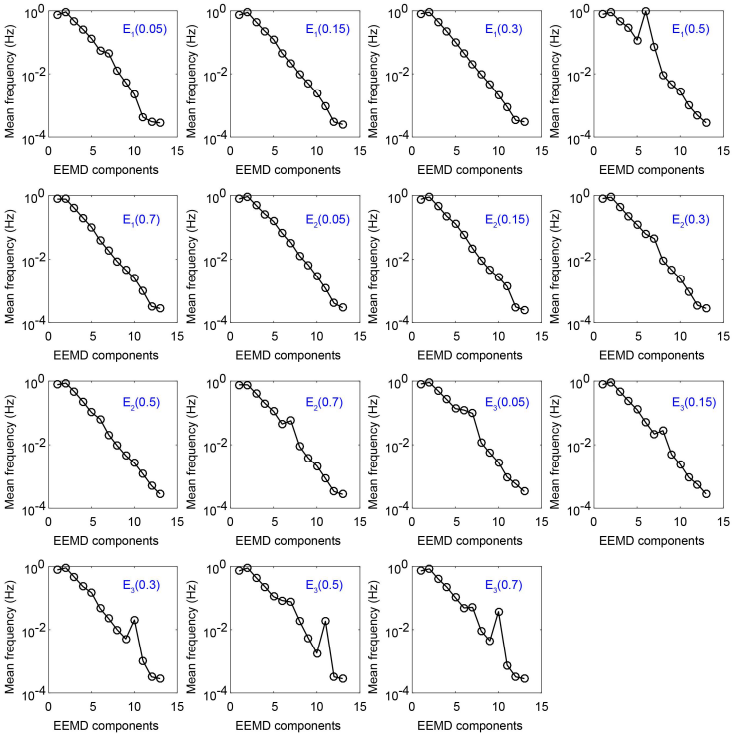

Figure S6. The mean frequencies of IMFs ξ_1-ξ_{13} for 3-D E-fields at all measurement points, $E_1 - E_3$ from 0.05 to 0.7 m height.

Please see page 10 in the revised Supplement for details.

Comments 02: a) The reduction of height z to the dimensionless z* is dependent on the saltation height, which is determined from measured SPC-91 data. I understood that SPC-91 is a particle counter that gives number size distribution. How was the mass information obtained from this data? What assumptions you made? How do the measurement uncertainties and assumptions influence the estimated saltation height? Does the saltation height vary with time?

b) It is described in section 4.1 that 'normalized vertical component E3* increases monotonically as height increases in the saltation layer'. However, in fig. 5c, the data points clustering at z* between 0.5 and 1 showed lower E3* than the ones at smaller z*. Therefore, this statement is not valid. It also seems that data points at z*=1-1.5 are always deviated from the trends in Figs. 5a-c. What could be the reason?

c) The authors used hourly bins in Fig. 5. How will the patterns look like if finer bins are used, e.g. 30 min or 10 min?

Response:

Our responses for this comment are threefold:

a) In fact, the SPC measures the particle number passing through the measurement area per second in the range of 30-490 μm with 64 bins, as shown in Fig. R1. That is to say, it measures the particle number flux with 64 given bins. If the particle mass density is known, we can estimate the mass flux based on the SPC data (please see Text S1 in the Supplement for details). The detailed estimation of mass flux from SPC data can be also found in the following reference:

"Mikami, M., Yamada, Y., Ishizuka, M., Ishimaru, T., Gao, W., & Zeng, F. (2005). Measurement of saltation process over gobi and sand dunes in the Taklimakan desert, China, with newly developed sand particle counter. Journal of Geophysical Research: Atmospheres, 110(D18)."

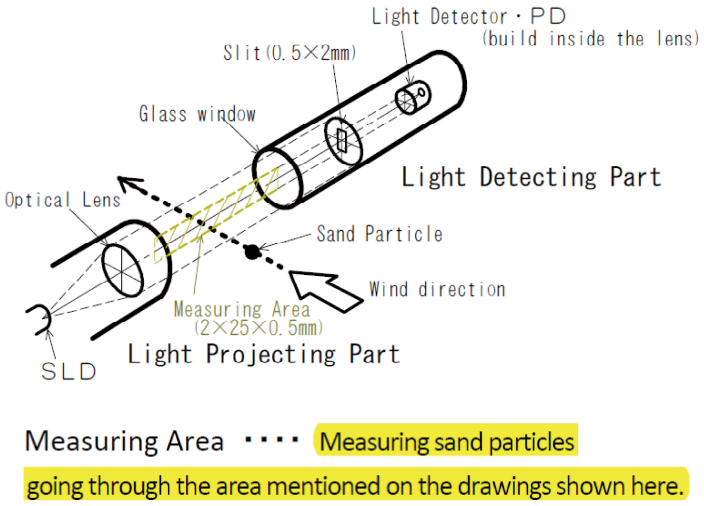

Figure R1. Schematic diagram of the measuring principle of SPC-91, which is redrew based on the "*SPC-91 Installation Guide, Niigata Electric Co., Ltd.*"

Because SPC measures the particle diameter with uncertainty of $\Delta d = \pm 0.015$ mm *(SPC-91 Installation Guide, Niigata Electric Co., Ltd.)*, the uncertainty of estimating mass flux is $\Delta q \sim 3d^2\Delta d$ (i.e. $q \sim d^3 \Rightarrow \Delta q \sim 3d^2\Delta d$). The measured mass flux profiles are shown in Fig. S2 (see below). As discussed in the Text S1 in the Supplement, the saltation height can be approximated as a function of the fitted parameter a:

$$z_{salt} = -\frac{\ln(0.01)}{a} \qquad (R1)$$

where the measured mass flux profile is excellently fitted by the exponential function $q(z) = q_0 \exp(-az)$.

According to Eq. R1, the uncertainty of z_{salt} can be estimated as:

$$\Delta z_{salt} = \frac{\ln(0.01)}{a^2}\Delta a \qquad (R2)$$

where Δa is the 95% confidence bounds.

It is worth noting that in the revised MS, mass flux q is estimated over every 30-

min time intervals, in order to collect sufficient sand sample and capture the full range of turbulent fluctuations (see Martin and Kok, 2017 and Sherman and Li, 2012 for the details). Fig. S3 shows the comparison of the mass flux and z_{salt} estimated by three different time intervals. It can be seen that there is no obvious difference between the mean values but the standard deviation decreases with increasing time interval. Fig. S3 shows the estimated saltation height. We can see that z_{salt} slightly varies with time and can be approximately considered as a constant, which is also verified in the previous studies in the case of steady-state saltation (Kok et al., 2012; Martin and Kok, 2017). In the revised MS, the height z is normalized by the mean saltation height $\bar{z}_{salt}$, because it could obtain a better representation of the E-field profiles (Fig. 5in the revised MS).

For comments 02 a), the following changes have been made in the revised Supplement:

"…In our field campaign, we measured the saltating particle number flux at 6 heights from 0.05 to 0.7 m. Thus, the mass flux at each measurement height can be reasonably estimated by

$$q(z) = \frac{\pi \rho_p}{6 L_x L_y T_w} \sum_{i=1}^{n} (N_i d_i^3) \qquad \text{(s2)}$$

Note that the summation $\sum$ is performed for the particles located in the range of $[z, z + \Delta z]$ over the 30-min time windows (i.e., T_w=30 minutes), in order to collect sufficient sand samples and capture the full range of turbulent fluctuations (e.g. Martin and Kok, 2017; Sherman and Li, 2012). Since SPC-91 measures the particle diameter with an uncertainty of $\Delta d = \pm 0.015$ mm (see SPC-91 Installation Guide, Niigata Electric Co., Ltd. for details), the uncertainty of estimating mass flux is $\Delta q \sim 3d^2 \Delta d$ (i.e. $q \sim d^3 \Rightarrow \Delta q \sim 3d^2 \Delta d$). As shown in Fig. S2, the measured mass flux data during different time intervals can be well fitted by the exponential functions (Shao, 2008):

$$q(z) = q_0 \exp(-az) \tag{s3}$$

where q_0 is the value of q at $z = 0$ and a is a positive empirical constant. Hence, the total mass flux can be determined by

$$Q = \int_0^{+\infty} q(z)dz = \frac{q_0}{a} \tag{s4}$$

Similarly, the uncertainty of the total mass flux is

$$\Delta Q = \frac{a\Delta q_0 - q_0 \Delta a}{a^2} \tag{s5}$$

Additionally, the saltation height, which is defined as the height below which 99 % of the total mass flux is present, can be given by (Dupont et al., 2013; Kok et al., 2012)

$$\int_0^{z_{salt}} q(z)dz = \frac{0.99 q_0}{a} \tag{s6a}$$

$$\Rightarrow z_{salt} = -\frac{\ln(0.01)}{a} \tag{s6b}$$

Similarly, the uncertainty of the saltation height is

$$\Delta z_{salt} = -\frac{\ln(0.01)}{a^2} \Delta a \tag{s7}$$

As shown in Fig. S3, the estimated saltation height slightly varies with time, and thus we use the mean saltation height, which is 0.172 $\pm$ 0.0343 m, to obtain the dimensionless height z^+. For different time windows (i.e. T_w =5, 10, 30 minutes), there is no obvious differences between the mean values of Q and z_{salt}, but the

standard deviations decrease as T_w increases (Fig. S3). Please see pages 2-4 in the revised Supplement for details.

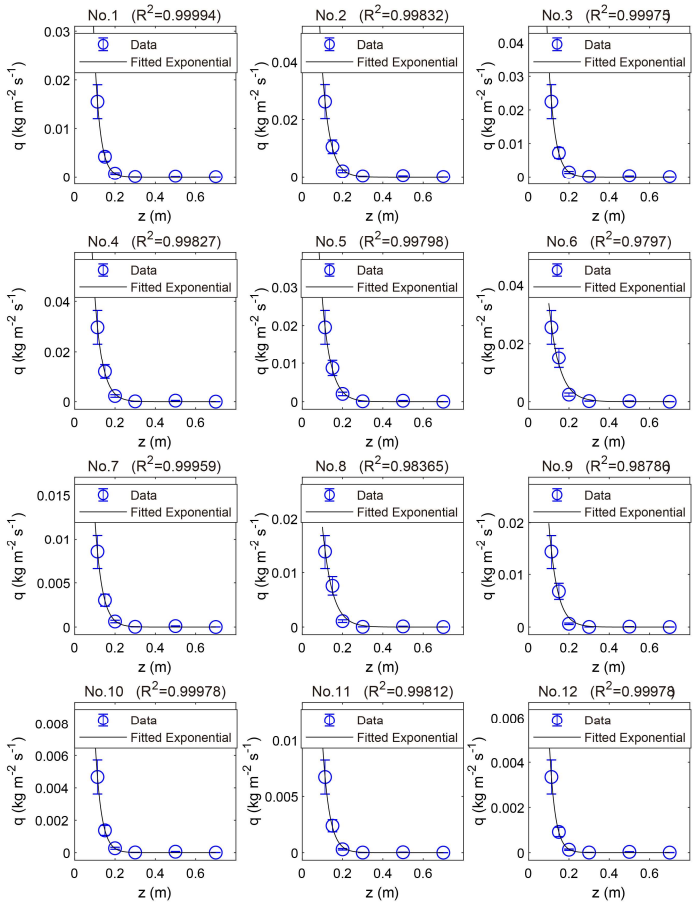

Figure S2. An example of the estimation of the total mass flux Q and saltation height z_{salt} in this study, where No. i corresponds to time interval of $[(i-1)T, iT]$. The measured mass flux data are fitted by the exponential function $q(z) = q_0 \exp(-az)$, with R^2 larger than 0.9. Thus, the total mass flux and saltation height can be estimated by Eqs. s4-s7 in the Supplement, respectively. Please see page 6 in the revised Supplement for details.

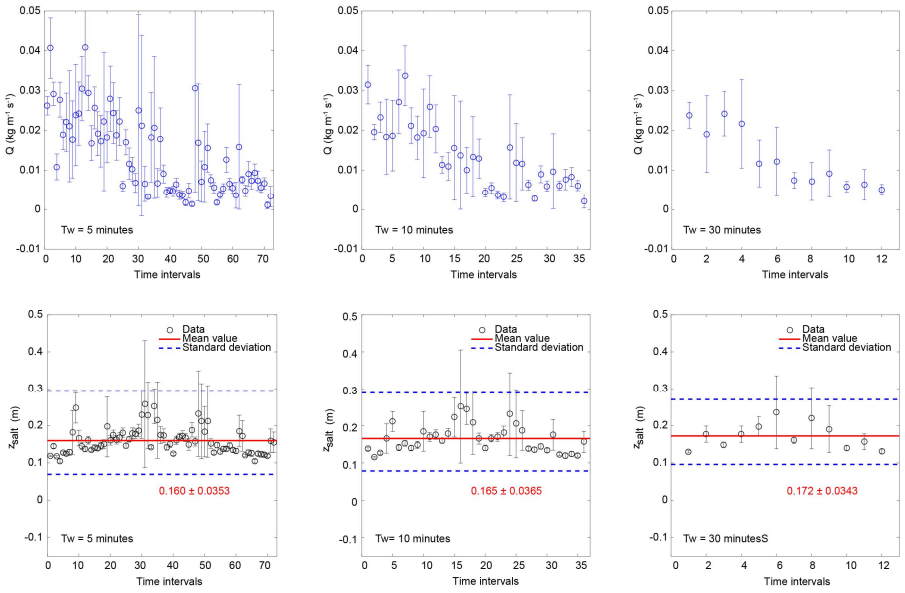

Figure S3. The estimated total mass flux Q (upper panels) and the saltation height z_{salt} (lower panels) with different time windows T_w (i.e. 5, 10, and 30 minutes) using the methods described in the Text S1. In the lower panels, the horizontal lines (in red) denote the mean saltation height, and the horizontal dashed lines (in blue) denote standard deviation. The shaded areas denote the relatively steady period of the observed dust storm.

Please see page 7 in the revised Supplement for details.

b) In the original MS, the heights z are normalized by z_{salt} in each time interval (1 h), thus leading to the data points at z*=1-1.5 are always deviated from the trends. By contrast, in the revised MS, because the heights z are normalized by the mean saltation height $\bar{z}_{salt}$ (a constant), these exist only five dimensionless heights z^+ (which, in turn, correspond to five measurement points) in Fig. 5. As shown in the Fig. R2 (redrawn from Figure 5 in the revised MS), at each measurement point, all data are horizontally distributed.

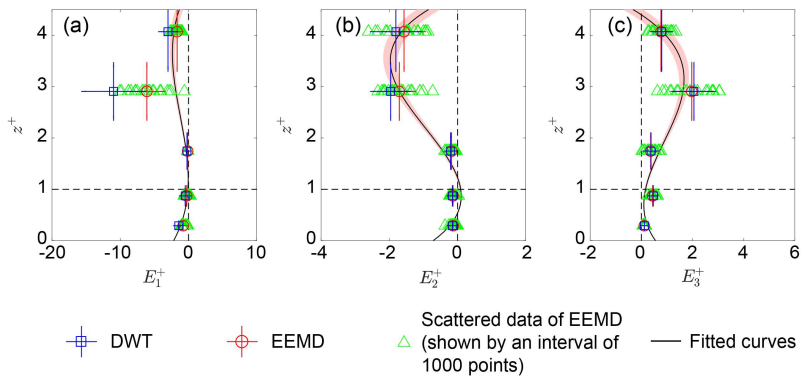

Figure R2 (redrawn from Figure 5 in the revised MS). Vertical profiles of the normalized 3-D E-field. Subgraphs (a)-(c), in turn, correspond to the vertical profiles of E_1^+, E_2^+, and E_3^+ of the observed dust storm. Squares and circles denote the DWT mean and EEMD mean values of the normalized E-field data, respectively. Triangles denote the scattered data of EEMD, which are shown by an interval of 1000 points (that is the first, 1001-th, 2001-th… points are shown). Error bars are standard deviations. Lines denote robust linear least-squares fitting of the normalized E-field data obtained by DWT and EEMD method using 3-order polynomials (with R^2 of 0.77, 0.78, and 0.93, respectively), where the shaded areas denote 95% confidence bounds.

In addition, from Fig. R2, we can see that the fitted vertical component curve decreases monotonically with increasing height when z^+ is less than 1. Therefore, in the revised MS, we have modified the statement of "normalized vertical component E3* increases monotonically as height increases in the saltation layer" as:

"… Interestingly, Fig. 5c shows that during dust storms, all normalized components, E_1^+ to E_3^+, decreases monotonically as height increases in the saltation layer (i.e. $z^+ \leq 1$), similar to the pattern of vertical component in pure saltation…" Please see page 19 lines 21-23 in the revised MS for details.

c) In the revised MS, when exploring the 3-D E-field pattern, we do not use time window (hourly bins in the original MS) to analyze E-field series. That is, for an E-field component at a given height [e.g. $E_3(t, 0.5)$ series], there are a total of 21,600 dimensionless E-field data points (i.e. all data points during 6 hours) E_3^+ used to fit the 3-order polynomial function, as shown in Fig. R2. Therefore, in the revised MS we do not explore (not required) the effects of time window (e.g. 10 or 30 minutes) on E-field pattern.

Comments 03: The authors considered midair particle-particle collisions with a viscoelastic force model in the saltation model to stimulate particle motion. This inclusion of the midair particle-particle interaction is shown to be important. However, during midair particle-particle interaction, particle diameters may change upon collision or frictional contact, e.g. due to cleavage of agglomerates, which may increase

the total number of particles in the system and shift the size and charge distributions of the particle population. Have the authors thought about these effects?

Response:

In our model, we do not consider particle agglomeration and fragmentation during collisions. According to your comment, we have added the discussions about particle agglomeration and fragmentation:

"However, a remaining critical challenge is still to simulate particle triboelectric charging in dust storms precisely. The driving atmospheric turbulent flows having a typical Reynolds number on the order of 10^8 cover a broad range of length and time scales, which needs huge computational cost to resolve (e.g. Shao, 2008). On the other hand, particle triboelectric charging is so sensitive to particle's collisional dynamics that it needs to resolve each particle collisional dynamics (e.g. Hu et al., 2012; Lacks and Sankaran, 2011). To model the particle's collisional dynamics properly, the time steps of DEM are generally from 10^{-7} to 10^{-4} s (Norouzi et al., 2016). However, steady-state saltation motion often requires several seconds to several tens of seconds to reach the equilibrium state. In this study, when $u_* = 0.5$ m s^{-1} and the computational domain is 0.5×0.1×1.0 m^3, the total number of saltating particles exceeds 7×10^4 (Fig. S8 in the Supplement). Consequently, the triboelectric charging in saltation is currently very difficult to simulate, where a large number of polydisperse sand particles, the high Reynolds-number turbulent flow, and the inter-particle electrostatic forces are mutually coupled. In the present version of the model, we do not consider the particle-particle interactions such as particle agglomeration and fragmentation during particle collision or frictional contact, as well as the particle-turbulence interaction that is the effects of turbulent fluctuations on the triboelectric charging and dynamics of particles. Further studies require considerable effort to incorporate these interactions, especially turbulence, which is very important for large wind velocity." Please see page 25 lines 1-20 in the revised MS for details.

Comments 04: The authors performed a simple sensitivity study of mass flux on the

effects of E-field intensity factors. It is said that the red curve corresponds to the observed dust storm. Where did the authors obtain the intensity factors for the other two cases? Are they realistic compared to reported observations in literature?

Response:

In the original MS, λ is actually the height-averaged time-varying mean of the E-field $\langle\overline{E_i}\rangle$, which is clearly defined by Eq. 5 in the revised MS. To eliminate the ambiguous meaning of λ, we directly regard the height-averaged time-varying mean as a basic parameter in the revised MS (therefore λ has been removed). The determination of $\langle\overline{E_i}\rangle$ is clearly shown in section 2.2 of the revised MS, namely:

"… Here, we use the discrete wavelet transform (DWT) method (Daubechies, 1990) and the ensemble empirical mode decomposition (EEMD) method (Wu and Huang, 2009), which are widely used in various geophysical studies (e.g. Grinsted et al., 2004; Huang and Wu, 2008; Wu et al., 2011), to estimate the time-varying mean values of the measured non-stationary 3-D E-field data. We select these two methods since the DWT with higher orders of Daubechies wavelet (e.g. db10) and the EEMD can extract a reasonable and physically meaningful time-varying mean (Su et al., 2015). Each step for revealing the 3-D E-field pattern is described in detail as follows:

The DWT uses a set of mutually orthogonal wavelet basis functions, which are dilated, translated and scaled versions of a mother wavelet, to decompose an E-field series $E(t,z)$ into a series of successive octave band components (Percival and Walden, 2000), i.e.,

$$E(t,z)=\sum_{i=1}^{N}\psi_i(t,z)+\chi_N(t,z) \tag{1}$$

Where N is the total number of decomposition levels, $\psi_i(t,z)$ denotes the i-th level wavelet detail component, and $\chi_N(t,z)$ represents the N-th level wavelet approximation (or smooth) component. As N increases, the frequency contents become lower and thus the N-th level approximation component could be regarded

as the time-varying mean values (e.g. Percival and Walden, 2000; Su et al., 2015). In this study, the DWT decomposition is performed with the Daubechies wavelet of order 10 (db10) at level 10, and thus the 10-th order approximation component can be defined as the time-varying mean:

$$\overline{E}(t,z) = \chi_{10}(t,z) \tag{2}$$

which reflect the averages of the $E(t,z)$ series over a scale of 2^{10} s (about 17.1 minutes).

On the other hand, according to the empirical mode decomposition (EMD) method, the time series $E(t,z)$ can be decomposed as (Huang et al., 1998)

$$E(t,z) = \sum_{i=1}^{N} \xi_i\,(t,z) + \eta_N(t,z) \tag{3}$$

through a sifting process, where $\xi_i(t,z)$ $(i = 1, 2, \dots, N)$ are the intrinsic mode functions (IMFs), and $\eta_N(t,z)$ is a residual (which is the overall trend or mean). To reduce the end effects and mode mixing in EMD, the EEMD method is proposed by Wu and Huang (2009). In EEMD, a set of white noise series, $w_j(t,z)$ $(j = 1,2, \dots N_e)$, are added to the original signal $E(t,z)$. Then, each noise-added series is decomposed into IMFs followed by the same sifting process as in EMD. Finally, the i-th EEMD component is defined as the ensemble mean of the i-th IMFs of the total of N_e noise-added series (see Wu and Huang, 2009 for details).

In this study, the time-varying mean values $\overline{E}(t,z)$ can be alternatively defined as the sum of the last four EEMD components, $\xi_{10}(t,z)$ to $\xi_{13}(t,z)$, and the residual, $\eta_{13}(t,z)$, i.e.

$$\overline{E}(t,z) = \sum_{i=10}^{13} \xi_i(t,z) + \eta_{13}(t,z) \tag{4}$$

which is approximately the 17.3 minutes (very close to the timescale of ~17.1 minutes used in DWT) or longer timescale variability trend (Wu et al., 2011), because the maximum mean frequency of the last four EEMD components is 5.78 $\times 10^{-2}$ Hz (see Figs. S5 and S6 in the Supplement for details).

According to the above definitions, the time-varying mean can be obtained by the DWT and EEMD methods over the timescale of about 17 minutes. As an example, Fig. 2 shows the results of db10 DWT analysis (Fig. 2b) and EEMD decompositions (Fig. 2c) for an E-field time series $E(t,z)$ in our field campaign. It can be seen that DWT and EEMD can properly capture the time-varying mean over the timescale of 17 minutes, with very little difference between the two methods.

Since the 3-D E-field are measured at five heights in our field campaign, we thus define the height-averaged time-varying mean values as

$$\langle \overline{E_i}(t,z) \rangle = \left| \frac{1}{(0.7-0.05)} \int_{0.05}^{0.7} \overline{E_i}(t,z) dz \right| \quad (5)$$

in the range of 0.05 to 0.7 m height, in order to normalize the E-field data by a unified quantity.…" Please see pages 6-8 in the revised MS for details.

Therefore, the height-averaged time-varying mean (i.e. intensity factors in the original MS) can be obtained by above methods. The height-averaged time-varying means of the observed dust storm are shown in Fig. S7 in the revised Supplement. So far, since there is no other multi-points measurement of 3-D E-field during dust storms, we cannot compare our results with other data in the literature.

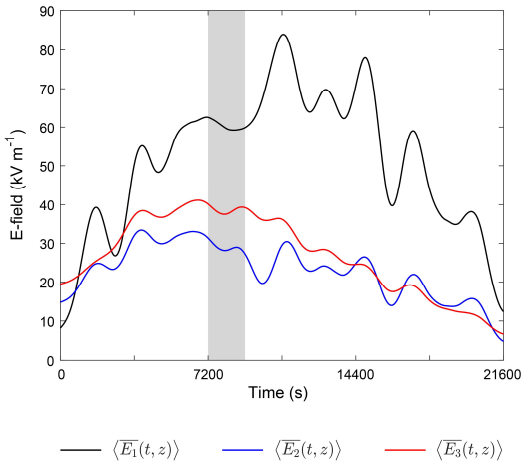

Figure S7. The height time-varying mean series of the 3-D E-field. The shaded area denotes the relatively steady period of the observed dust storms. Times are shown relative to May 6, 2014 at 13:00:00 UTC+8.

Please see page 11 in the revised Supplement for details.

Comments 05: This study is based on one case. It therefore lacks the statistics to reach statements, like 'This 3-D E-field model successfully resolves the discrepancy between the 1-D E-field model (e.g. Kok and Renno, 2008) and the recent measurement (i.e. Esposito et al., 2016).' or 'The DEM implemented by cell-based algorithms is robust enough to detect and evaluate all particle-particle midair collisional dynamics.' Two aspects here:

a) It is weak in reaching conclusions based on a single case study. Also for model validation purpose, it would be important to apply the algorithms to at least another case. It will largely improve the quality and strength of the results, if the authors could add a second case to support.

b) The 3-D E-field model indeed shows a good agreement with observations, but the discrepancy between the 1-D E-field model and measurement may not only be due to the exclusion of the two other dimensions of the E-field. It is good that the authors took into consideration of particle-particle midair collisional dynamics in the model, but what the authors implemented in the model certainly do not account for all. I would like to suggest the authors make a revision of the language in sections 5.3, 5.4

and 6 to avoid exaggeration in discussing the methods and results as well as conclusions drawn therefrom.

Response:

Unfortunately, we have only observed one dust storms in the 2014 field campaign since the occurrence of dust events are highly stochastic. As you pointed out that, the properties of dust storms may vary from event to event. Thus, in the revised MS, we have added the following discussions in section 5.1:

"…Additionally, the 3-D E-field pattern of dust storms may vary event to event, because it is strongly related to the driving mechanisms of dust storms, such as monsoon winds, squall lines, and thunderstorms (Shao, 2008), and ambient conditions, such as temperature and relative humidity (Esposito et al., 2016; Zhang and Zheng, 2018). Although the 3-D E-field pattern revealed in this study may not be a universal feature, the proposed E-field data analysis method can be easily applied to other cases." Please see page 23 lines 2-8 in the revised MS for details.

In addition, according to your suggestion, we have modified the language in sections 5.3, 5.4 and 6 in order to avoid exaggeration. The main reversions are as follows:

In section 5.3:

"… The DEM implemented by cell-based algorithms is effectively to detect and evaluate most of the particle-particle midair collisional dynamics (Norouzi et al., 2016) …"

Please see page 24 lines 8-10 in the revised MS for details.

In section 5.4:

"…This 3-D E-field model may resolve the discrepancy between the 1-D E-field model (e.g. Kok and Renno, 2008) and the recent measurement (i.e. Esposito et al., 2016)…"

Please see page 24 lines 26-27 in the revised MS for details.

In section 6:

"…(2) the inclusion of 3-D E-field in saltation model may resolve the discrepancy between previous 1-D E-field model (e.g. Kok and Renno, 2008) and measurements (Esposito et al., 2016) in the aspect of whether the E-field inhibits or enhances saltation…"

Please see page 26 lines 3-6 in the revised MS for the details.

Comments 06: P20 line 26: remove explicitly; 7. P20 line 28: It does not seem to me that the 3-order polynomial curves can capture the patterns well in Fig. 5. Therefore, it is inappropriate to say '… providing a detailed characterization…'

Response:

According to your suggestion, we have modified the statement "…we explicitly account for the particle-particle tribo-electrification during midair collisions in saltation…" as

"…we account for the particle-particle triboelectric charging during midair collisions in saltation…"

Please see page 24 lines 7-8 in the revised MS for details.

We have modified the statement "…providing a detailed characterization of the 3-D E-field during dust storms for the first time…" as

"…providing a simple representation of the 3-D E-field during dust storms for the first time…"

Please see page 26 lines 2-3 in the revised MS for details.